AIAA SciTech
5-9 January 2015, Kissimmee, Florida
33rd Wind Energy Symposium

AIAA 2015-0489

SAND2015-7509C

# Analysis of the Impact of Leading Edge Surface Degradation on Wind Turbine Performance

Christopher M. Langel*, Raymond Chow†, Owen F. Hurley‡, and C.P. van Dam§
*University of California, Davis, Davis, CA 95616*

Robert S. Ehrmann¶ and Edward B. White‖
*Texas A&M University, College Station, TX 77843*

David Maniaci**
*Sandia National Laboratories, Albuquerque, NM 87185*



**Over time it has been reported wind turbine power output can diminish below manufacturers promised levels. This is clearly undesirable from an operator standpoint, and can also put pressure on turbine companies to make up the difference. A likely explanation for the discrepancy in power output is the contamination of the leading edge due to environmental conditions creating surfaces much coarser than intended. To examine the effects of airfoil leading edge roughness, a comprehensive study has been performed both experimentally and computationally on a NACA $63_3-418$ airfoil. A description of the experimental setup and test matrix are provided, along with an outline of the computational roughness amplification model used to simulate rough configurations. The experimental investigation serves to provide insight into the changes in measurable airfoil properties such as lift, drag, and boundary layer transition location. The computational effort is aimed at using the experimental results to calibrate a roughness model that has been implemented in an unsteady RANS solver. Furthermore, a blade element momentum code was used to assess the impact on the performance of a turbine as whole due to discrepancies in clean vs. soiled airfoil characteristics. The results have implications in predicting the power loss due to leading edge surface roughness, and can help to establish an upper bound on admissible surface contamination levels.**

## I. Introduction

### A. Motivation

Optimal performance of wind turbine blades is critical to insuring cost effective power delivery. Aerodynamic behavior plays a dominant role in overall efficiency, giving rise to highly refined blade profiles designed to maximize energy capture. However, with increased performance comes increased sensitivity to changes in design conditions. One of the changes observed is the contamination of the leading edge due to insect and soil buildup, paint chipping, and erosion of the surface over time. Images taken from in field turbines can be seen in Figure 1. A well-known effect of a rough surface is the acceleration of the laminar-turbulent transition process.[1] The early introduction of a turbulent boundary layer can have a number of undesirable consequences by altering lift and stall characteristics. The changes in the flow over degraded portions of a turbine blade can effect the performance of the full turbine, potentially reducing power output and annual energy capture significantly.[2]

*Graduate Student Researcher, AIAA Student Member.
†Postdoctoral Scholar, AIAA Member.
‡Graduate Student Researcher.
§Professor & Chair, Associate Fellow AIAA.
¶Graduate Research Assistant, AIAA Student Member.
‖Associate Professor, Associate Fellow AIAA.
**Senior Member of Technical Staff.

The inclusion of roughness sensitivity to airfoil and full turbine design poses numerous challenges due to the limited number of roughness configurations that have been thoroughly analyzed, and the non-trivial extension of roughness effects. As physically testing each airfoil profile in varying rough configurations is not practical, numerical optimization methods are used to generate ideal airfoils and other flow control surfaces. However, there are limited computational techniques available to analyze the effects that surface roughness will have on the aerodynamic properties.[3,4] Typically, to estimate the impact surface degradation may have, 2-D trip strips are used to generate a turbulent boundary layer near the leading edge. This procedure intends to mimic the premature transition to turbulence observed over rough surfaces. Experiments have also illustrated that random distributed roughness is not properly simulated by trip strips, raising questions regarding the use of such techniques to simulate surface contamination.

Historically, surface roughness effects were a problem for constant speed, stall-controlled wind turbine rotors. However, the introduction of variable speed , variable pitch, pitch to feather rotors mitigated many of these effects and with that, surface roughness appeared to be a problem of the past. The wind industry has seen a recent rise in the effects of surface roughness for several reasons.[3] First, the wind industry has matured and now continuously tracks turbine and plant performance. Roughness-induced performance effects can lead to unanticipated loss in plant capacity factors with obvious financial consequences.[5] Second, turbine design has changed in that turbines have become larger and more optimized to maximize their aerodynamic performance while minimizing the growth in blade weight. These design changes include higher lift-to-drag section shapes in the outboard region, and thicker section shapes in the inboard region with the aerodynamic performance of both being more sensitive to surface roughness. Moreover, the effects of roughness may be further amplified over the outboard region of the blade. For example, blade erosion may be more predominant in this region where the local flow velocity is higher because this causes more energetic impacts with soiling or eroding elements. This is further exacerbated by the relatively greater impact the outboard region has on overall rotor performance.

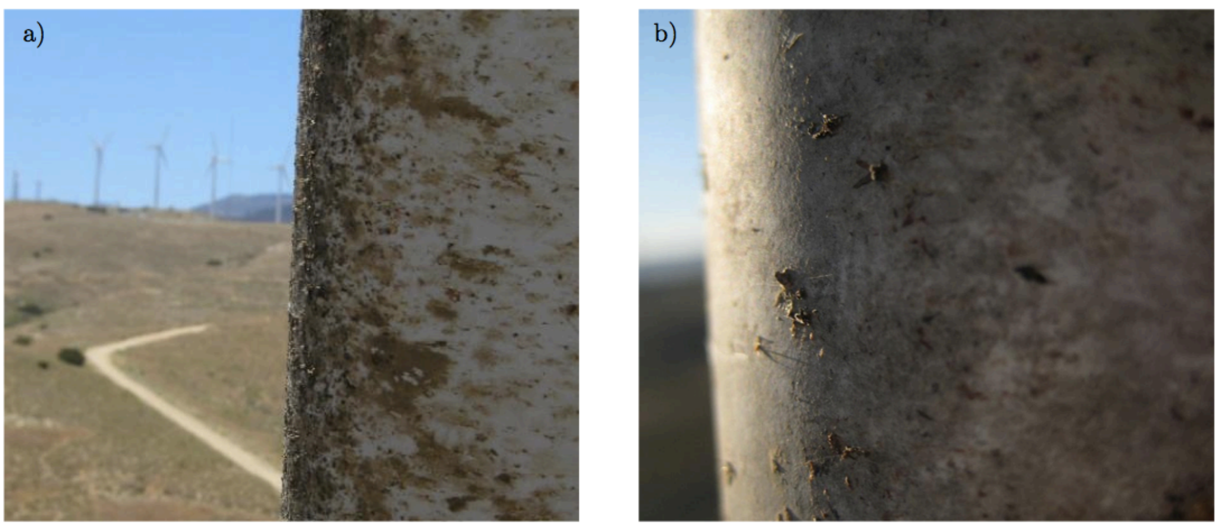


**Figure 1. Images of insect roughness on leading edges from a) Spruce[5] and b) the current work.**

To further understand the impact distributed roughness may have on airfoil characteristics a collaborative effort has been undertaken by groups at UC Davis, Texas A&M University, and Sandia National Laboratories. An extensive wind tunnel testing campaign was conducted on a NACA $63_3 - 418$ airfoil at Texas A&M. The tests included a variety of different roughness heights and distribution densities, all at a wide range of angles of attack and Reynolds numbers. For the purpose of both prediction of flows over existing rough surfaces and roughness insensitive designs, a robust computational method that predicts the effects of various surface roughness distributions is strongly desired. Accordingly, concurrent to the experimental investigation a computational model is being developed at UC Davis to predict the effects of roughness on both transition and the developing turbulent boundary layer. The model is calibrated to the results of the experimental study with the hope further of extending its validity to untested configurations, allowing for use in a predictive capacity and in the design process itself.

### B. Roughness Effects

A crucial component is characterization of the roughness parameters such as the height, shape, and distribution. All must all be taken into consideration to fully understand the effects. The relationship between the height of the roughness element and the flow disturbance induced is not easily correlated.[6] Roughness elements shorter than the height of the viscous sublayer generally have little effect on the transition process as the disturbances are dissipated away due to the high levels of viscous damping. Additionally as the boundary layer does not have a constant thickness, the effects cannot be generalized along the boundary layer of a rough surface.[7] Accordingly, roughness heights are usually non-dimensionalized with respect to the displacement thickness ($k/\delta^*$) or described using a roughness Reynolds number, $Re_k$. The roughness Reynolds number is defined:

$$Re_k = \frac{\rho U_k k}{\mu} \tag{1}$$

where $U_k$ represents the velocity in an undisturbed boundary layer at the roughness height, $k$. Due to the $U_k$ term, even if the height of the roughness remains constant, $Re_k$ will change along a surface as the boundary layer develops. Frequently, experimental studies have attempted to identify a critical Reynolds number, $Re_{k,crit}$.[9] This represents the value of $Re_k$ that if obtained on a rough surface will immediately trigger the transition process at that location. As many external factors such as freestream turbulence, acoustic noise, and crossflow contamination can alter transition characteristics, $Re_{k,crit}$ values inherently contain some uncertainty.

Roughness distributions can be broadly classified into three different subsets: 2D roughness (such as a trip strip or step), isolated 3D rough element, and distributed roughness, encompassing any grouping of rough elements and inherently 3D. Different types of roughness are known to alter the transition process uniquely, and therefore have differing $Re_{k,crit}$ values. 2D roughness is known to amplify the naturally occurring Tollmien-Schlichting wave dominated transition process by introducing a Rayleigh instability, and can act to progressively move the transition location upstream.[10] Isolated 3D roughness introduces flow structures known as horseshoe and hairpin vortices. These vortices remain relatively stable and have little effect on the transition process until the height of the roughness reaches a point where transition location moves rapidly upstream.[11] Due to this phenomena, isolated 3D roughness is considered to behave more "critically" than 2D. Isolated 3D roughness elements have an $Re_{k,crit}$ between 400-600 depending on the shape and height to diameter ratio.[11]

Distributed roughness becomes more difficult to quantify, one height parameter ($k$) is no longer enough to fully describe the roughness and its respective effects on the transition process. Several attempts have been made to correlate measurable parameters to an "equivalent" sand grain roughness heights ($k_s$). A review conducted by Bons[12] provides the details of many efforts to create an equivalent $k_s$ value given certain quantifiable parameters. Furthermore, the exact mechanism by which distributed roughness alters transition characteristics remains misunderstood. Several conjectures have been made as to how distributed roughness promotes the transition process. These include streamwise vortex structures produced in a similar manner to isolated 3D elements, increased receptivity of the low inertia fluid in between the rough elements, and vertical transfer of $u$-momentum altering the mean profile. Despite challenges in identifying exactly how the transitions process is accelerated $Re_{k,crit}$ values of $\sim 600$ for distributed roughness have been used to a reasonable degree of accuracy.[1]

## II. Experimental Setup and Test Configurations

The wind tunnel experiments were conducted at the Texas A&M Oran W. Nicks Low Speed Wind Tunnel (LSWT). The LSWT is a closed-return tunnel with a 7 ft $\times$ 10 ft test section that can achieve freestream velocities of 90 m/s. For the given test conditions, the wind tunnel has a turbulence intensity of 0.25% and excellent flow uniformity. The wind tunnel has an external balance beneath the test section to which the model is mounted. The section shape selected, NACA $63_3 - 418$ is a typical outboard airfoil for utility-scale wind turbines. The chord is 0.813 m, yielding 4.8% blockage, and 2.1 m in span (model aspect ratio = 2.6). In order to achieve unique roughness configurations, the model was designed to be modular with a removable leading edge at 15% chord. Two piano hinges along the upper and lower main body are used to securely attach the leading edge. The hinge pins can be removed through holes in the wind tunnel wall, allowing simple model changes while creating a stiff interface between the leading edge and airfoil main body. The model was manufactured from aluminum, ensuring minimal deflections at maximum load. The model mounted vertically with approximately 12.5 mm of clearance at the ceiling and floor. Pitch variation is achieved by rotating the floor balance. Many measurements were made to characterize the airfoil performance. Lift and moments were calculated by integrating surface pressure measurements. Drag was determined from a wake survey. Lastly, transition location was indicated with IR thermography, further details regarding measurement techniques are provided by Ehrmann and White.[13,14]

To assess the impact of distributed roughness, numerous different roughness configurations were tested. The roughness was simulated by generating randomly distributed circles in a $152.3 \times 152.3$ mm$^2$ area using circles with a normally distributed radius of $1.2 \pm 0.15$ mm. If a circle happens to intersect another circle, an ellipse is circumscribed around the two circles such that its area is minimized. If any object remains overlapped, it is removed. Objects are randomly removed to create different coverage densities, and the pattern is repeated in the spanwise direction such that the whole model is covered. To create the patterns on the airfoil leading edge, each was etched into a vinyl decal such that the circles and ellipsoids are placed on the model as rough features. The roughness pattern extends from 2% chord on the upper surface to 13% on the lower in accordance with observation and the ice accretion code NASA LEWICE.[15] An example of the pattern and placement can be seen in Figure 2 (b). Vinyl of varying thickness was used to create roughness of different heights; tested in the experiment were $100\mu m$, $140\mu m$, and $200\mu m$. This range of heights allowed a large range of $Re_k$ values to be observed.

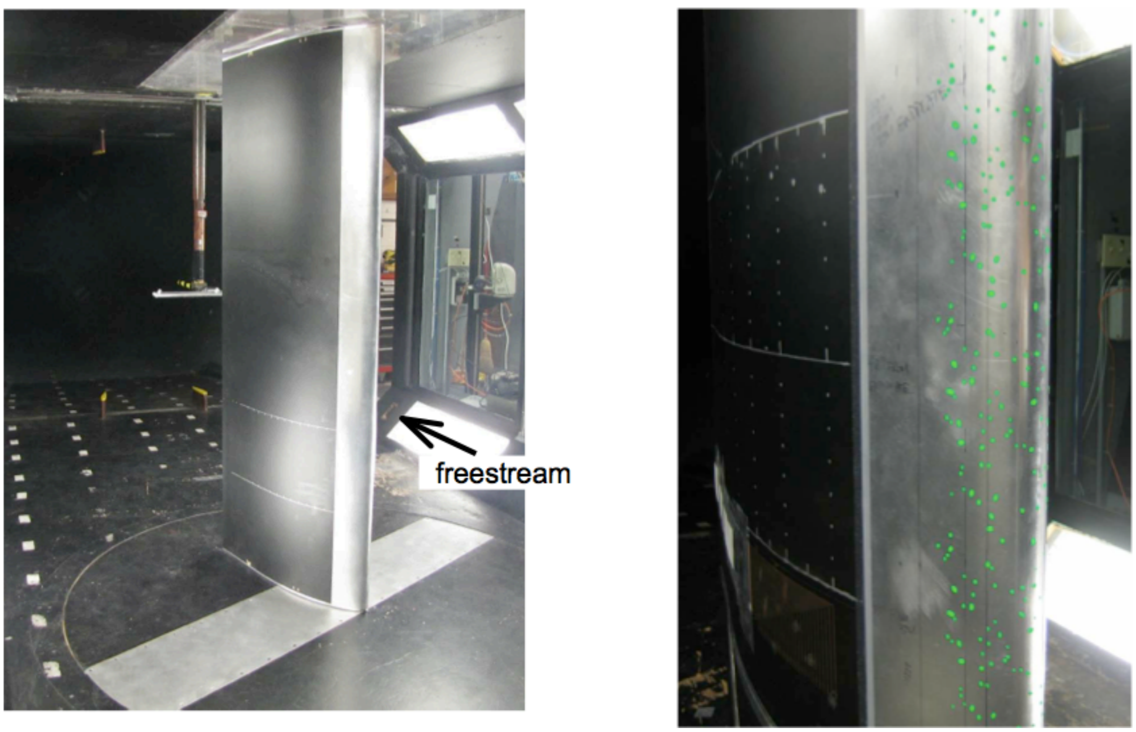


**Figure 2. (left) Clean model mounted in the LSWT, (right) close up of the leading edge with an example of the roughness pattern used.**

In addition to height variation, differences in coverage density and chordwise extent were tested. Table 2 provides a summary of the various height and density distributions, while Figure 3 gives a representation of the patterns used.

**Table 1. Summary of tested distributed roughness configurations**

| Height | Densities (%) | Extent |
|---|---|---|
| 100 $\mu$m | 3, 9, 15 | 2% chord on upper to 13% lower surface |
| 140 $\mu$m | 3, 6, 9, 12, 15 | 2% & 6% chord on upper to 13% lower surface |
| 200 $\mu$m | 3, 15 | 2% chord on upper to 13% lower surface |

Each of the configurations was tested at a Reynolds number of 0.8, 1.6, 2.4, 3.2, 4.0 and 4.4 $\times 10^6$ with angles of attack varying from $-4^o$ to $16^o$. At higher Reynolds numbers, the floor balance will overload so the upper angle of attack was limited to $+6^o$ at $4.0 \times 10^6$ and $+4^o$ at $4.4 \times 10^6$. Reynolds number sweeps were also completed at $0^o$ and $6^o$ angles of attack.

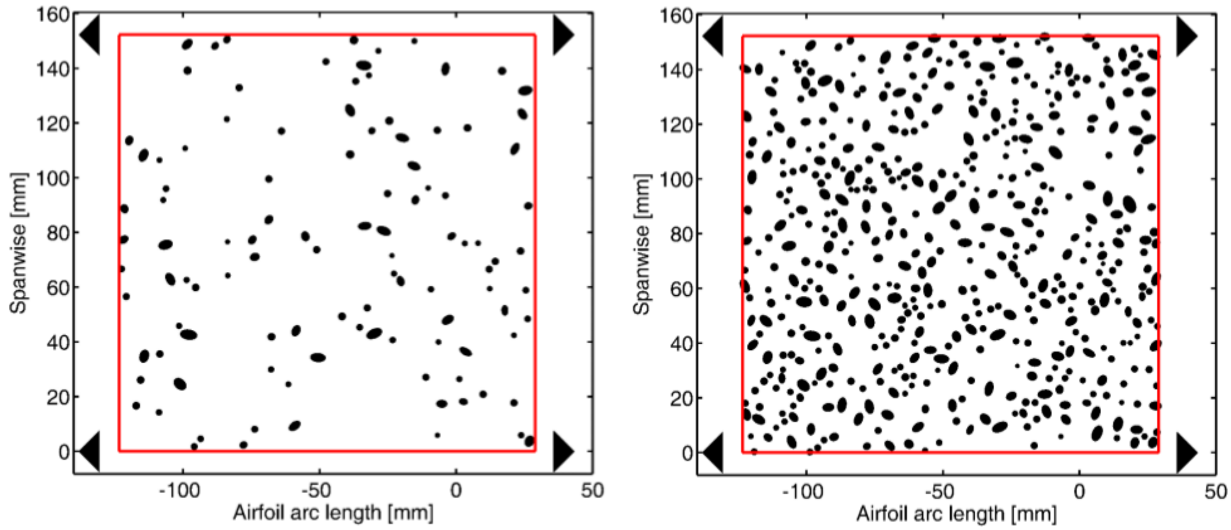


**Figure 3. Example of roughness configuration pattern showing density variation, left 3%, right 15%.**

Throughout the course of the experimental study it was observed that both roughness height and distribution density can affect how significantly the roughness impacts the flow. Figure 4 shows how variation in both of these variables impacts drag at a chord Reynolds number of 2.4 and 3.2 million.

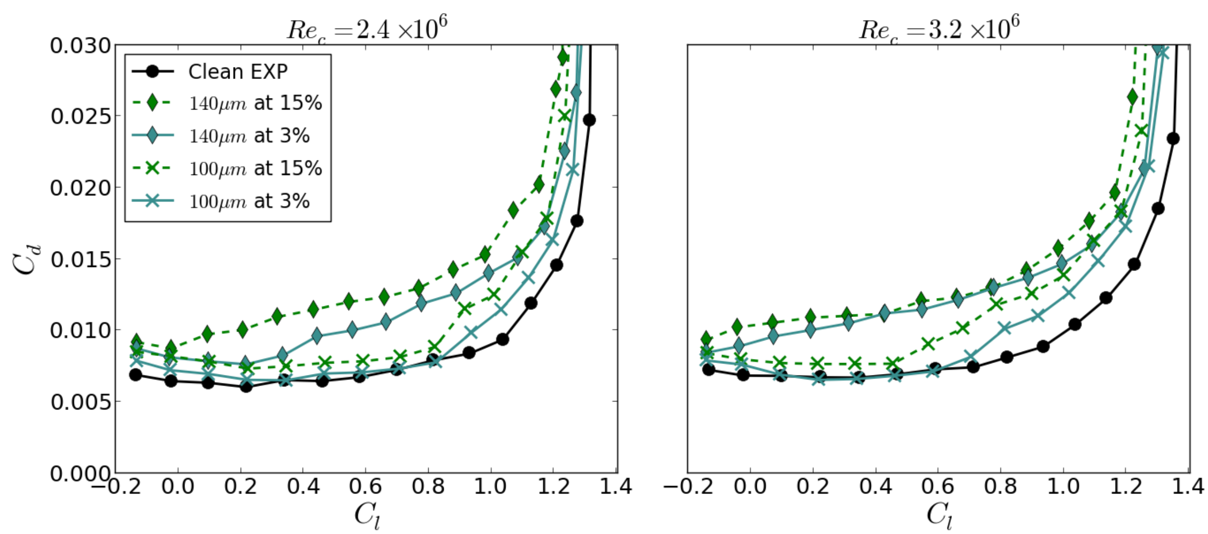


**Figure 4. Impact of variation of both roughness height and distribution density, NACA $63_3 - 418$, all cases roughness applied from $x/c = -0.13 : 0.02$.**

An observation from Figure 4 is that as the Reynolds number is increased, the drag predictions show less sensitivity to changes in distribution density at $140\mu m$ height. The behavior does begin to deviate again at higher $C_l$ values, implying that an airfoil designed with a high lift-to-drag ratio may experience more effects than a single height parameter may suggest. Nonetheless, it is clearly import to characterize the roughness distribution both in terms of height and coverage density to adequately capture the effects on airfoil performance.

# III. Computational Methodology

A common engineering approach to analyzing complex flow problems is the use of Reynolds-averaged Navier-Stokes (RANS) simulations. Fundamentally RANS procedures require the use of a complementary closure or turbulence model to fully represent practical flows. Unfortunately these models fail to account for many physical mechanisms that cause a boundary layer to transition from laminar to turbulent. This is not easily corrected as many factors can ultimately cause the breakdown of a laminar boundary layer into a characteristic turbulent form. Nonetheless, a recently developed approach is that of local correlation-based transition modeling (LCTM).[16,17] The general concept is to introduce an empirically correlated quantity based on freestream values that is subsequently compared to local flow conditions and used to indicate transition onset. A primary appeal of LCTM is that these methods are designed to predict boundary layer transition entirely based on local flow quantities allowing parallelization and use on unstructured grids.[17]

## A. Langtry-Menter $\gamma - \tilde{R}e_{\theta t}$ Model

An increasingly popular local correlation model is the Langtry-Menter $\gamma - \tilde{R}e_{\theta t}$ model. It introduces two non-physical flow parameters that work in conjunction with one another to determine the criteria the local flow has to meet to induce transition, and once triggered, ramp up to the fully turbulent state.[16,17] The first of the two variables the Langtry-Menter transition model relies on is referred to as "intermittency" ($\gamma$). It differs from the physically defined parameter of the same name in that it does not represent the exact turbulent state of the boundary layer but acts as a scaling parameter. Within a laminar boundary layer the intermittency variable shuts off the production of turbulent kinetic energy ($k$) and once local criteria are met, it is used to progressively activate $k$ production. The second variable is defined as the "transition onset momentum thickness Reynolds number" ($\tilde{R}e_{\theta t}$). It is designed to take an empirical correlation based on freestream turbulence intensity and local pressure gradient and introduce local effects using a transport equation. The quantity $\tilde{R}e_{\theta t}$ is compared to other local flow quantities and used to trigger intermittency production and subsequent ramping of turbulent kinetic energy, attempting to mimic the physical transition process. Two transport equations are used to define the distribution of $\gamma$ and $\tilde{R}e_{\theta t}$ and are defined,

$$\frac{\partial(\rho\gamma)}{\partial t} + \frac{\partial(\rho U_j \gamma)}{\partial x_j} = P_\gamma - E_\gamma + \frac{\partial}{\partial x_j}\left[\left(\mu + \frac{\mu_t}{\sigma_f}\right)\frac{\partial \gamma}{\partial x_j}\right] \tag{2}$$

$$\frac{\partial(\rho\tilde{R}e_{\theta t})}{\partial t} + \frac{\partial(\rho U_j \tilde{R}e_{\theta t})}{\partial x_j} = P_{\theta t} + \frac{\partial}{\partial x_j}\left[\sigma_{\theta t}\left(\mu + \mu_t\right)\frac{\partial \tilde{R}e_{\theta t}}{\partial x_j}\right] \tag{3}$$

The production term within the intermittency equation ($P_\gamma$) is a strong function of ($\tilde{R}e_{\theta t}$). Also included is an explicit destruction term ($E_\gamma$ ), to account for the possibility of relaminarization. The term $P_{\theta t}$ is used to modify the freestream empirical correlation according to local flow conditions. A more detailed description, and full equation set is presented by Langtry & Menter.[17]

## B. Surface Roughness Considerations

Following the recent rise in popularity of local correlation transition models, several researchers have sought to incorporate roughness correlations into LCTMs. Notably, Stripf et al.[18] and Elsner & Warzecha[19] both proposed a direct modification of the transition onset criteria based on roughness height and displacement thickness ($\delta^*$). A similar approach to modeling roughness taken by Dassler, Koluvic, & Fiala[20] was to introduce a field quantity governed by an additional transport equation that defines a region of roughness influence. The scalar field is then used to modify the transition onset criteria. A similar "roughness amplification" method is used in the current study with the introduction of an additional scalar variable ($A_r$) and corresponding transport equation. The equation takes the form:

$$\frac{\partial(\rho A_r)}{\partial t} + \frac{\partial(\rho U_j A_r)}{\partial x_j} = \frac{\partial}{\partial x_j}\left[\sigma_{ar}\left(\mu + \mu_t\right)\frac{\partial A_r}{\partial x_j}\right] \tag{4}$$

The $A_r$ transport equation does not include an explicit production term, alternatively the distribution of $A_r$ is determined with a boundary condition at rough walls where the user inputs a representative equivalent sand grain roughness height ($k_s$). The primary factor influencing the value of $A_r$ at rough walls is the dimensionless roughness variable, $k^+$. Defined:

$$k^+ = \sqrt{\frac{\tau_w}{\rho_w}} \cdot \frac{k_s}{\nu} \quad (5)$$

The value of $A_r$ at the rough wall boundary is then defined as a function of $k^+$ based on empirical calculations. Further details and the full equation set are provided in Langel et al.[22,23]

For this study the aforementioned roughness amplification model has been implemented in OVERFLOW-2. For all cases the primary flow variables are calculated with sixth-order central differencing using the approximate-factorized form of the Beam-Warming pentadiagonal scheme.[24] The spatial fluxes of the roughness model are discretized using a modified Harten-Lax-van Leer (HLLC) upwind scheme as extension of the existing Langtry-Menter model with the linear matrix solved using a similar successive symmetric over relaxation (SSOR) algorithm.

As a demonstration of the capacity of the model, results are provided comparing the models prediction to a few of the cases described in Figures 5 and 6. The roughness configuration for comparison was the $140\mu m$ height at the highest density tested, 15%. As mentioned both roughness height and distribution density must be considered when parameterizing the roughness configuration. At the highest density, the equivalent sand grain input to the model, $k_s$, is the dimensionless height of the roughness $k/c$. It is presumed that at the highest density, the roughness introduces disturbances most similar to a "sand grain roughness" of the same height. As shown in the Figures 5 and 6 the model does a good job predicting the changes to both transition location and drag due to leading edge roughness.

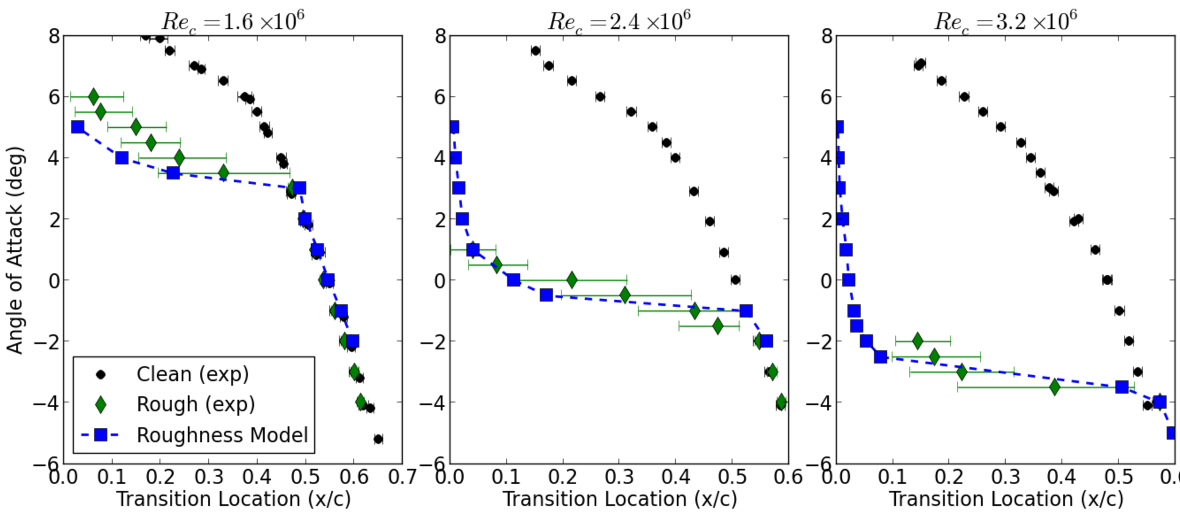


**Figure 5. Comparison of upper surface transition location prediction compared to experimental results, NACA $63_3-418$, $k/c = 172 \times 10^{-6}$ ($140\mu m$) roughness applied from $x/c = -0.13 : 0.02$, distribution density 15%. $k_s = 172\mu m$ input into roughness model.**

## IV. NREL 5-MW

To assess the impact of surface degradation on the performance of a wind turbine rotor as a whole, the roughness model was applied to geometry from the NREL 5-MW turbine. Six different airfoil profiles were analyzed in both a "clean" and "rough" configuration using OVERFLOW-2 and the roughness amplification model described. New airfoil tables were created that correspond to the both the unmodified and soiled conditions. Although there are no experimental studies to compare the soiled airfoil performance with, the outboard span of the turbine utilizes a similar profile to the NACA $63_3 - 418$ tested. With the accuracy of the predictions from the model shown, it is not unreasonable to use the model in its current formulation. Additionally, there is no single roughness distribution that the study is attempting to match, more the effects of soiling in general. Figures 7 and 8 provide the drag polar and $C_l - \alpha$ curve for a representative outboard and midspan airfoil. The lowering of both stall angle and $C_l$ max due to roughness is apparent for both airfoils. A consistent increase in drag is also observed across all $C_l$ values.

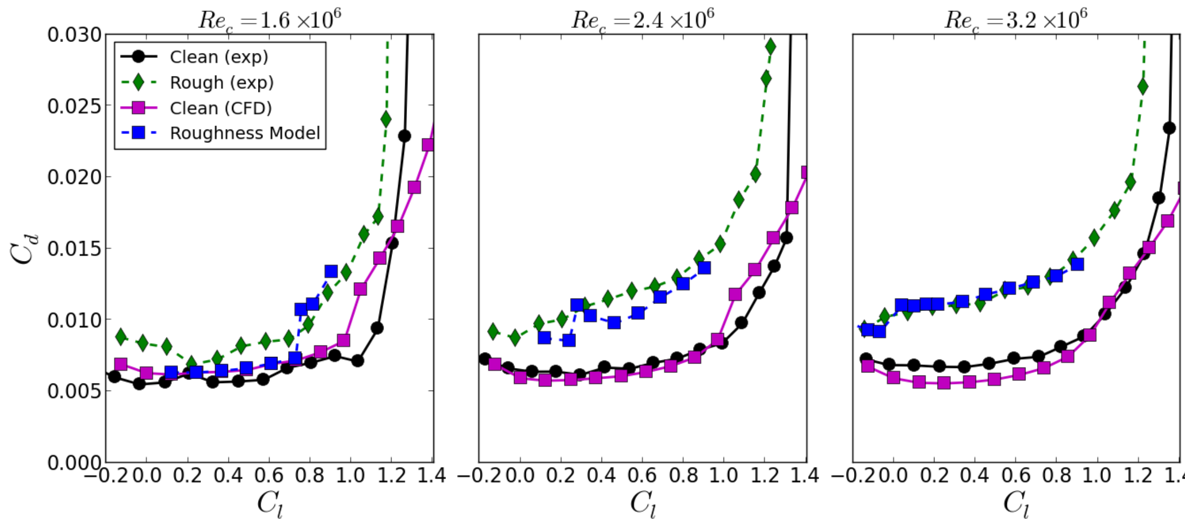


**Figure 6. Predicted drag polars compared to experimental results, NACA $63_3-418$, $k/c = 172 \times 10^{-6}$ $(140\mu m)$ roughness applied from $x/c = -0.13 : 0.02$, distribution density 15%. $k_s = 172\mu m$ input into roughness model.**

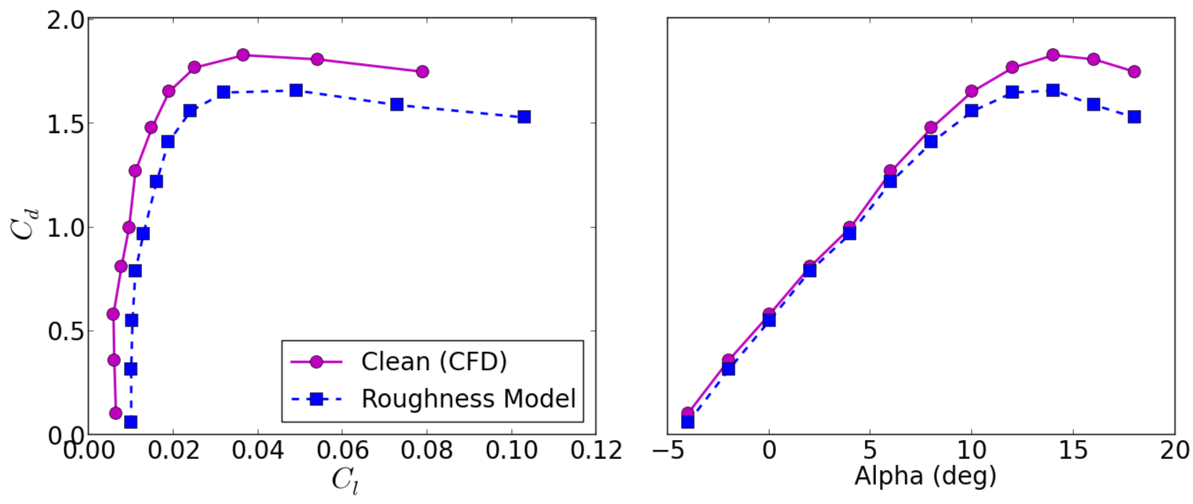


**Figure 7. Drag polar and $C_l - \alpha$ curve for outboard NACA 64-618 airfoil, $Re_c = 8.59 \times 10^6$, $k_s = 240\mu m$ roughness applied from 5% chord lower to 5% chord upper surface.**

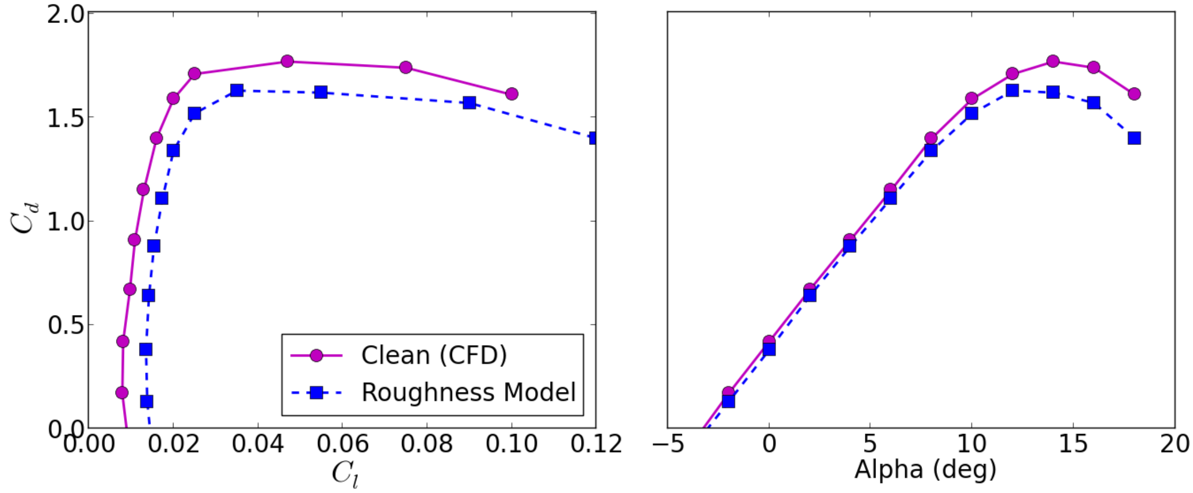


**Figure 8. Drag polar and $C_l - \alpha$ curve for midspan DU-91-W210 airfoil, $Re_c = 7.24 \times 10^6$, $k_s = 240\mu m$ roughness applied from 5% chord lower to 5% chord upper surface.**

Table 2 is provides a summary of the impacts of roughness on airfoil performance characteristics as determined by the experimental study (NACA $63_3 - 418$) and application of the roughness model to the NREL 5-MW airfoils.

**Table 2. Impact of roughness on airfoil performance**

| Case | Reduction in max $C_l$ | Reduction in max $L/D$ |
|---|---|---|
| 140 $\mu$m at 15% (exp) | -7% | -42.0% |
| DU-97-W-300 (CFD) | -9.8% | -20.2% |
| DU-91-W2-250 (CFD) | -7.9% | -23.7% |
| DU-93-W-210 (CFD) | -15.2% | -24.8% |
| NACA 64-618 (CFD) | -8.3% | -34.0% |

The NREL airfoils are given in order of their spanwise placement on the turbine, with the DU-97-W-300 closest to the hub and the NACA 64-618 furthest outboard. All of the computational runs utilize the roughness model with an input $k_s$ of $240\mu m$ with the extent of the roughness covering the first 5% chord on both the upper and lower surfaces. The experimental case provided should behave closest to the NACA 64-618 and indeed the computational model predicts similar changes to maximum lift and lift-to-drag ratio. An interesting trend is the increasing impact on max $L/D$ as the airfoils move from the root of the blade to the tip. The thicker inboard airfoils appear to be less sensitive to roughness in terms of max $L/D$, however, the drop in max $C_l$ appears slightly larger.

WT-Perf was used to predict the performance of the clean and soiled rotor. WT-Perf is a steady-state horizontal axis wind turbine performance analysis tool developed by the National Renewable Energy Laboratory's National Wind Technology Center (NWTC). WT-Perf provides simple and fast analysis of rotor performance. WT-Perf utilizes Blade Element Momentum (BEM) theory to predict rotor performance through the use of discreet and independent annular sections in the spanwise direction of the blade. BEM makes the following critical assumptions:

1. No aerodynamic interactions occur between elements.
2. The forces acting on the blades are exclusively determined by the lift and drag characteristics of the element.

These assumptions allow WT-Perf to predict aerodynamic forces along the rotor using local flow conditions and two-dimensional airfoil data. These forces are then summed along the blade span to calculate the total forces and moments acting on the rotor. No attempt is made by WT-Perf to model the flexure in the rotor and thus the program assumes that the rotor is infinitely stiff. In addition to these assumptions, WT-Perf assumes that the flow field is free of turbulence and is constant along the horizontally plane. Wind shear can be included in the analysis using a power law relation, but was not included in this study. Although WT-Perf is capable of analysis of turbines with constant yaw error the accuracy of the analysis has not been verified and the flow was assumed to be perpendicular to the rotor. Tip and hub losses are modeled using a Prandlt loss factor. An iterative approach is then used to calculate the forces produced on the rotor blade via Blade Element analysis and the forces produced by moment theory until the solution converges.

For each radial element, the chord length and pitch is defined and provided with data relating $C_l$ and $C_d$ versus angle of attack. Separate tables were used to replicate the clean and rough rotor conditions. A combined case analysis was used to predict rotor power at both clean and rough conditions. In the analysis input, blade pitch and rotor speed are tabulated as a function of wind speed. The pitch schedule was created such that power was maximized until rater power was reached. Power output was maximized at a pitch angle of zero degrees and thus until rated power is reached, the pitch angle is constant. The rotor speed schedule was held constant at the design conditions for the NREL 5-MW.[26] The roughness model does have the capacity to be applied to a 3-D simulation of the full rotor, however for the present study, BEM was an effective and efficient option.

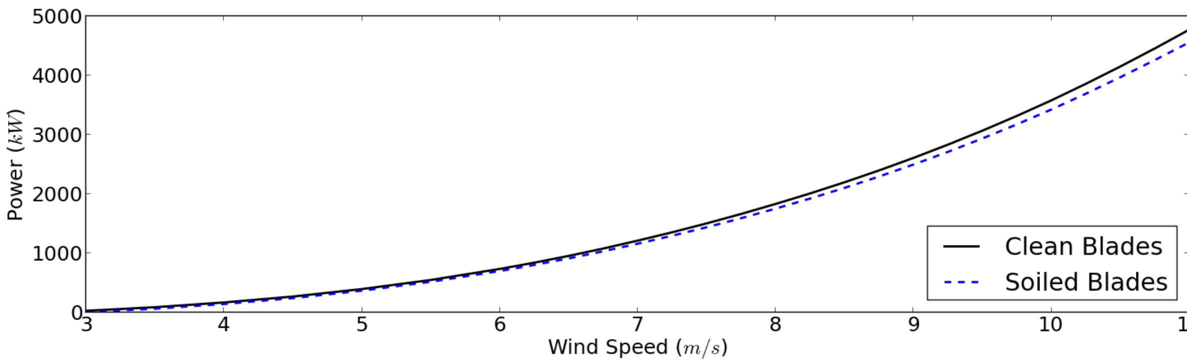


**Figure 9. Predicted effect of leading edge roughness on region II power curve for NREL 5-MW ($k_s = 240\mu m$ applied from 5% chord lower to 5% chord upper surface for each component airfoil).**

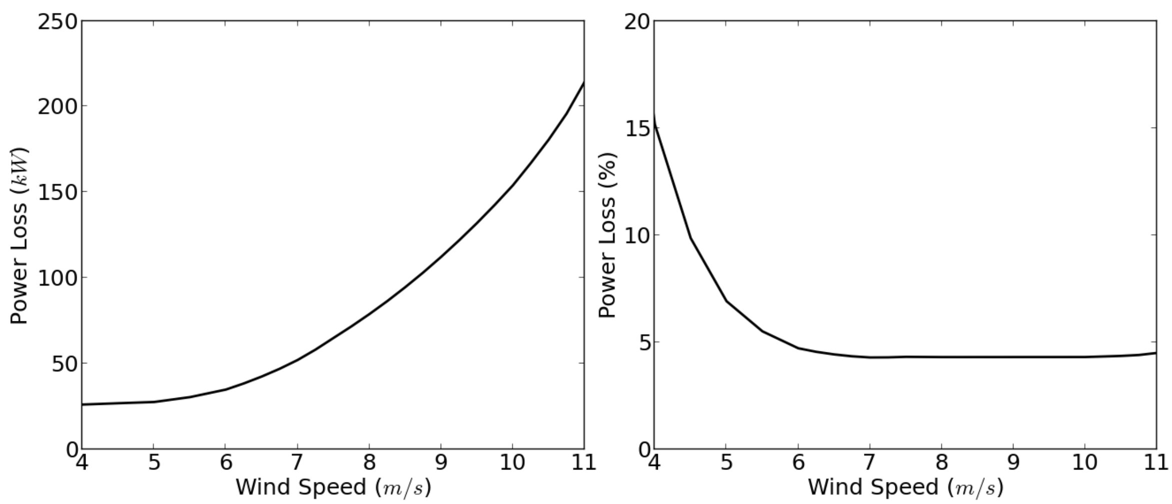


**Figure 10. Predicted power loss due to leading edge roughness for NREL 5-MW ($k_s = 240\mu m$ applied from 5% chord lower to 5% chord upper surface for each component airfoil).**

The results show discrepancies primarily in region II of the power curve. This is to be expected as the turbine will operate in a constant pitch configuration, meaning changes in sectional lift characteristics will have a direct impact on power output. It can be seen in Figure 10 that the predicted power loss is roughly 5% across the mid to upper range of region II. Once in region III, the pitch scheduling can be changed such that a soiled turbine can operate at peak power, however it is projected the lowering of stall angle and $C_l$

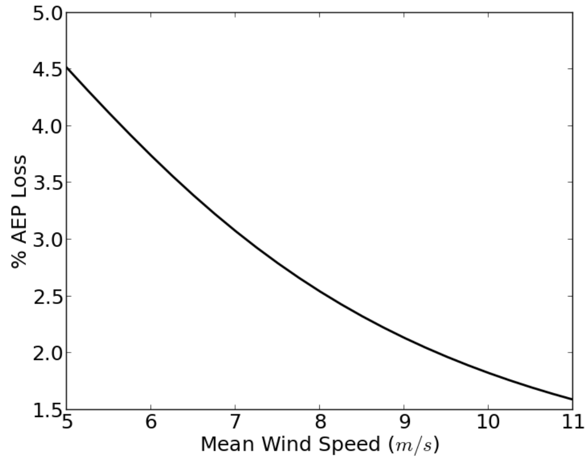


**Figure 11. Predicted AEP loss for NREL 5-MW due to leading edge roughness ($k_s = 240\mu m$ applied from 5% chord lower to 5% chord upper surface for each component airfoil).**

max may affect highly optimized blades.

To provide a better understanding of how the change in performance due to roughness will alter the energy capture of a turbine, a change in annual energy production (AEP) was computed for varying wind distributions. In accordance with IEC61400-12-1 guidelines, the power curves for both the rough and clean blades were applied to a Rayleigh wind speed distribution with a mean speed of 5 to 11 m/s. A minimum cut-in wind speed of 3 m/s was used, as well as the assumption the turbines would operate at a level output in region III. The percentage loss at each mean wind speed is plotted in Figure 11. At higher wind speeds the power loss is not as severe because the turbines are operating in region III for a higher percentage of time, where the blades are pitched to keep power output constant. The computed percentage loss in AEP is actually comparable what was observed by Ehrmann and White for an in field turbine with insect roughness.[25]

The NREL 5-MW rotor does not operate at a particularly high design lift coefficient, meaning it is fairly robust to changes in the upper portion of the lift curves of its component airfoils. However, as blades are pushed further into higher levels of performance, sections of the blade are pushed closer to their respective stall angle. This implies the changes seen due to roughness could alter the performance in a more dominant way through premature flow separation on the blade.

## V. Conclusions

A study to better understand the impact of leading edge blade contamination on wind turbine performance has been conducted. The effort has included both an extensive experimental campaign and development of a high fidelity simulation tool for analyzing the impact on roughness on flow properties. The wind tunnel tests have revealed the importance of both roughness height and distribution density in determining the extent to which surface degradation will affect the flow. Predictions from the computational roughness model show good agreement with the experimental results. Finally a demonstration of how the roughness model can be used to better calculate the effects of leading edge surface contamination on wind turbine power output was presented.

## Acknowledgments

The effort was performed for Sandia National Laboratories under contract number 1228734 (U.C. Davis) and 1209202 (TAMU) with David Maniaci and Matthew Barone as technical monitors. The work was additionally supported by the National Science Foundation GK-12 RESOURCE program under Grant No. DGE-0948021.

# References


[1]Corke, T.C., Bar-Sever, A., and Morkovin, M.V., " Experiments on Transition Enhancement by Distributed Roughness", *The Physics of Fluids*, Vol. 29, No. 10, 1986, pp. 3199-3213.

[2]Berg, D.E., "A Review of the Workshop on WECS Blade-Surface Roughness", *ASME Wind Energy Symposium*, 1993.

[3]Sareen, A. , Sapre, C.A., and Selig, M.S., "Effects of Leading Edge Erosion on Wind Turbine Blade Performance", *Wind Energy*, DOI: 10.1002/we.1649, 2013.

[4]van Rooij, R.P.J.O.M., and Timmer, W.A., "Roughness Sensitivity Considerations for Thick Rotor Blade Airfoils", *Journal of Solar Engineering*, Vol. 125, 2003, pp. 468-478.

[5]Spruce, C. J., "Power Performance of Active Stall Wind Turbines with Blade Contamination," *Proceedings of European Wind Energy Conference, EWEC*, Athens, 2006.

[6]Merkle, C.L., and Kubota, T., "An Analytical Study of the Effects of Surface Roughness on Boundary-Layer Transition", *Flow Research Inc Technical Report AD/A-004 786*, 1973

[7]Young, A.D., Paterson, J.H., and Jones, J.L., "Aircraft Excrescence Drag", *Aircraft Group for Aerospace Research and Development technical report No. 264*, 1981.

[8]Nikuradse, J., "Laws of Flow in Rough Pipes", *NACA Technical Report 1292*, 1933

[9]Braslow, A.L., and Knox, E.C., "Simplified Method for Determination of Critical Height of Distributed Roughness Particles for the Boundary-Layer Transition at Mach Numbers from 0 to 5", *NACA technical report 4363*, 1958.

[10]Klebanoff, P.S., and Tidstrom, K.D., "Mechanism by Which a Two-Dimensional Roughness Element Induces Boundary-Layer Transition", *The Physics of Fluids*, Vol. 15, No. 7, 1972, pp. 1173-1186.

[11]Acalar M.S., and Smith, C.R., "A Study of Hairpin Vortices in a Laminar Boundary Layer. Part 1. Hairpin Vortices Generated by a Hemisphere Protuberance", *Journal of Fluid Mechanics*, Vol. 175, 1987, pp. 1-41.

[12]Bons, J.P., "A Review of Surface Roughness Effects in Gas Turbines" *Journal of Turbomachinery*, Vol. 132, No. 021004, 2010, pp. 1-16.

[13]Ehrmann, R. S., White, E. B., Maniaci, D. C., Chow, R., Langel, C. M., van Dam, C.P., "Realistic Leading-Edge Roughness Effects on Airfoil Performance," *31st AIAA Applied Aerodynamics Conference* , June 24-27, 2013 , San Diego, California.

[14]Ehrmann, R. and White E. "Influence of 2D Steps and Distributed Roughness on Transition on a NACA $63_3 - 418$," *32nd ASME Wind Energy Symposium*, January 13-17, 2014.

[15]Wright, W.B., "User Manual for the NASA Glenn Ice Accretion Code LEWICE: Version 2.0," *NASA Technical Report*, NASA/CR-1999-209409, 1999.

[16]Menter, F. R., Esch T., and Kubacki, S., "Transition Modeling Based on Local Variables" *Proceedings of the 5th International Symposium on Engineering Turbulence Modelling and Measurement*, Elsevier, Amsterdam, 2002, pp. 555-564.

[17]Langtry, R. B., and Menter, F. R., "A Correlation-Based Transition Model for Unstructured Parallelized Computational Fluid Dynamics Codes," *AIAA Journal*, Vol. 47, No. 12, December 2009, pp. 2894-2906.

[18]M. Stripf, A. Schulz, H.J. Bauer, and S. Wittig, "Extended models for transitional rough wall boundary layers with heat transfer - part i: Model formulations, *Journal of Turbomachinery*, Vol. 131, No. 031016, 2009, pp. 110.

[19]W. Elsner, "Transition Modeling in Turbomachinery," *Journal of Theoretical and Applied Mechanics*, vol. 45, no. 3, pp. 539D556, 2007.

[20]Dassler P., Kozulovic D., and Fiala A., "Modeling of Roughness-Induced Transition Using Local Variables", in *European Congress on Computational Methods in Applied Sciences and Engineering (ECCOMAS 2012)*, September 10-14, 2012, Vienna, Austria

[21]Dassler P., Kozulovic D., and Fiala A., "Modeling of Roughness-Induced Transition Using Local Variables", in *V European Conference on Computational Fluid Dynamics*, June 14-17, 2010, Lisbon, Portugal.

[22]Langel, C.M, Chow, R., van Dam, C.P., Maniaci, D. C., Ehrmann, R. S. and White, E. B., "A Computational Approach to Simulating the Effects of Realistic Surface Roughness on Boundary Layer Transition", *52nd Aerospace Sciences Meeting*, January 13-17, 2014

[23]Langel, C.M, Chow, R., van Dam, C.P., "Further Developments to the Correlation Based Roughness Amplification Model," *53rd Aerospace Sciences Meeting*, January, 2015

[24]Beam, R., and Warming, R., "An Implicit Factored Scheme for the Compressible Navier-Stokes Equations," *AIAA Journal*, Vol. 16, No. 4, 1978, pp. 393402

[25]Ehrmann, R. and White E. "Seasonal Variation in Wind Turbine Power," *Wind Energy*, submitted, 2015.

[26]Jonkman, J., Butterfield, J., Musial, W., Scott, G., "Definition of a 5-MW Reference Wind Turbine for Offshore System Development," *National Renewable Energy Laboratory*, Golden, Colorado, 2009.

[27]Kerho, M. F., and Bragg M.,B., "Airfoil Boundary-Layer Development and Transition with Large Leading-Edge Roughness," *AIAA Journal*, Vol. 35, No. 1, Jan. 1997, pp. 75-84

[28]Dryden, H.L., "Combined Effects of Turbulence and Roughness on Transition", *ZAMP Zeitschrift fr Angewandte Mathematik und Physik*, Vol. 9, No. 5-6, 1958, pp. 249-258.

[29]van Ingen, J. L., "The $e^N$ method for transition prediction. Historical review of work at TU Delft," in *38th Fluid Dynamics Conference and Exhibit*, AIAA-2008-3830, June 23-26, 2008, Seattle, Washington.

[30]Brodeur, R. R., and van Dam, C. P., "Transition Prediction for a Two-Dimensional Reynolds-averaged-Navier-Stokes Method Applied to Wind Turbine Airfoils," *Wind Energy* 2001, 4, 61-75.

[31]Mayda, E.A., "Boundary-layer Transition Prediction for Reynolds-averaged Navier-Stokes Methods", Ph.D. Thesis, University of California, Davis, 2007

[32]Abu-Ghannam, B. J., and Shaw, R., "Natural Transition of Boundary Layers: The Effects of Turbulence, Pressure Gradient, and Flow History," *Journal of Mechanical Engineering Science*, Vol. 22, No. 5, 1980, pp. 213-228.

[33]Van Driest, E.R., and Blumer, C.B., "Boundary Layer Transition: Freestream Turbulence and Pressure Gradient Effects", *AIAA Journal*, Vol. 1, No. 6, 1963, pp. 1303-1306.

[34]Schubauer, G. B., and Klebanoff, P. S., "Contribution on the Mechanics of Boundary Layer Transition," NACA TN 3489, 1955.

[35]Jespersen, D. C., Pulliam, T. H., and Buning, P. G., "Recent Enhancements to OVERFLOW," *AIAA Paper 97-0644*, Jan. 1997.

[36]Spalart, P.R., and Rumsey, C.L., "Effective Inflow Conditions for Turbulence Models in Aerodynamic Calculations", *AIAA Journal*, Vol. 45, No. 10, 2007, pp. 2544-2558.

[37]Durbin, P.A., Medic, G., Seo, J.M., Eaton, J.K., and Song, S., "Rough Wall Modification of Two Layer $k-\epsilon$", *Journal of Fluids Engineering*, Vol. 123, 2001, pp. 16-21.

[38]Hellsten, A., and Laine, S., "Extension of the $k-\omega$ - SST Turbulence Model for Flows Over Rough Surfaces", *Proceedings of the AIAA Atmospheric Flight Mechanics Conference*, 1997.

[39]Aupoix, B., and Spalart, P., "Extensions of the Spalart-Allmaras Turbulence Model to Account for Wall Roughness," *International Journal of Heat and Fluid Flow*, vol. 24, no. 4, pp. 454-462, 2003.

[40]E. G. Feindt, "Untersuchungen ber die Abhngigkeit des Umschlages laminar- turbulent von der Oberflchenrauhigkeit und der Druckverteilung", DFL Bericht, 43 (1956)

[41]Wilcox, D. C., "Turbulence Modeling for CFD," DCW Industries, Second Edition, La Canada, California 1998.

[42]Ferrer, E., Munduate., "CFD Predictions of Transition and Distributed Roughness Over a Wind Turbine Airfoil", *47th AIAA Aerospace Sciences Meeting Including The New Horizons Forum and Aerospace Exposition*, AIAA-2009-0269, January 5-8, 2009, Orlando, Florida.

[43]Langtry, R. B., "A Correlation-Based Transition Model Using Local Variables for Unstructured Parallelized CFD Codes," Ph.D. Thesis, Univ. of Stuttgart, Stuttgart, Germany, 2006.